Tangent fermions: massless fermions on a lattice

Donís Vela, A.

CHAPTER 1

Introduction

1.1. Preface

A fundamental concept in condensed matter physics is that the effective behavior of electrons is strongly influenced by the medium in which they exist. An example of this is graphene, in which electrons are effectively massless. The symmetry of its celebrated honeycomb lattice imposes a band structure with two gap closings at two points in the Brillouin zone (BZ) [1, 2] around which the dispersion relation is a *Dirac cone* (Fig. 1.1)

$$E^2 = v^2(p_x^2 + p_y^2). \tag{1.1}$$

These points are called *Dirac points* and the Hamiltonian describing the low energy excitations around each of them is respectively

$$H_\pm = -i\hbar v(\partial_x \sigma_x \pm \partial_y \sigma_y). \tag{1.2}$$

This Hamiltonian realises the Dirac equation for massless fermions with velocity v in 2D, where the sign choice fixes the chirality of the particles.[1] The presence of two species of massless Dirac fermions with opposite chirality is not an accident but a consequence of a fundamental fact about

[1] For massless particles chirality and helicity coincide.

lattice Hamiltonians. Nielsen and Ninomiya [3] proved, in the context of high energy physics, that the following statements about a lattice Hamiltonian cannot be simultaneously true:

- The Hamiltonian is local.
- The Hamiltonian preserves chiral symmetry.
- The sum of chiralities of the Dirac points in the Brillouin zone is not zero.

This no-go theorem seems to imply that we cannot have a crystal with a single species of massless fermions. However, nature often manages to find a way around our expectations, and 3D topological insulators (3DTIs) are an example of this. These materials have a gapped bulk but a gapless surface whose low energy dispersion relation consists of a *single Dirac cone*. Nature is showing us that we can have a single species of massless chiral fermions as long as they are embedded in a lattice of larger dimension.

Yet, this does not mean that in order to simulate the 2D surface modes of a 3DTI we need to spend resources representing the whole 3D lattice. The problem of building a lattice model with a single Dirac cone is commonly referred to as the *fermion doubling problem* and it is well known in the field of lattice gauge theories where there have been many ways of tackling it [4–7]. The main part of this thesis focuses on addressing this problem within the framework of topological condensed matter by developing the *tangent fermions* approach, a scheme pioneered by Stacey that breaks the locality assumption [8].

The present chapter is dedicated to laying out some fundamental concepts related to the fermion doubling problem, as well as showing how 3DTIs can be used to build chiral superconductors and introducing the concept of non-Abelian braiding.

1.2. Topological protection of the Dirac cone and no-go theorem in 2D

Since disorder is unavoidable in real materials, we would like it to be accurately featured by our discretization scheme. One crucial trait of massless fermions on the surface of topological materials is the gapless nature of the Dirac cone even when disorder is present. This robustness is referred to as *topological protection*, and it relies on the presence of either

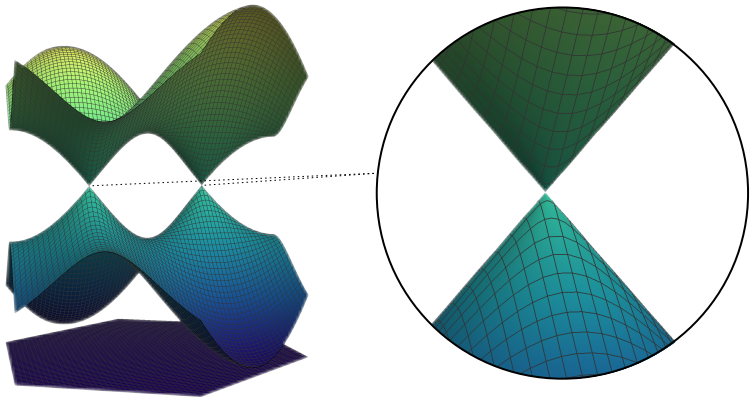

Figure 1.1: Band structure of graphene in the first Brillouin zone. Inset: Conical dispersion relation (Dirac cone) around the gap closings (Dirac points).

chiral or symplectic symmetries[2] but also on the Dirac cone to be the only one in the Brillouin zone.

In this section, we demonstrate how chiral and symplectic symmetries provide this topological protection for local Hamiltonians in 2D. By doing it, we also uncover the main obstacle to achieving it in a lattice model. Namely, that *a local discretization of the 2D Dirac Hamiltonian cannot have an unpaired Dirac cone, unless it breaks both chiral and symplectic symmetries.*

Chiral symmetry

A system has chiral symmetry if there exists a unitary and hermitian *chirality operator* Γ that anticommutes with the Hamiltonian. The conditions on Γ imply that it has two eigenspaces with eigenvalues ± 1 respectively and $\Gamma^2 = 1$. Also, the anticommutation with the Hamiltonian implies

$$\langle\psi_\pm| H |\phi_\pm\rangle = \langle\psi_\pm| \Gamma^2 H |\phi_\pm\rangle = -\langle\psi_\pm| \Gamma H \Gamma |\phi_\pm\rangle = -\langle\psi_\pm| H |\phi_\pm\rangle , \tag{1.3}$$

being $|\chi_+\rangle$ ($|\chi_-\rangle$) a state of positive (negative) chirality. So in the basis of eigenstates of Γ, the diagonal blocks of H are zero. We can then write

[2] Crystalline symmetries can also stabilize the Dirac point, in which case we talk about "fragile" topological protection [9].

our Hamiltonian by blocks as[3]

$$H(\boldsymbol{k}) = \begin{pmatrix} 0 & A^\dagger(\boldsymbol{k}) \\ A(\boldsymbol{k}) & 0 \end{pmatrix}. \tag{1.4}$$

Given a closed loop γ in the reciprocal space along which $\det A \neq 0$, we can define a *winding number* as

$$W = \frac{1}{2\pi} \operatorname{Im} \oint_\gamma \nabla_k \log\left(\det A(\boldsymbol{k})\right) \cdot d\boldsymbol{k}. \tag{1.5}$$

If the Hamiltonian is local, $A(\boldsymbol{k})$ is continuous and single valued. This implies that W must be integer and therefore we can use it as a topological invariant to classify Hamiltonians and loops. If there are no zeros of $\det A$ inside of γ, then the loop can be contracted to a point and $W = 0$.

From equation (1.2), it follows that at a Dirac point $\det A(\boldsymbol{k}_\mathrm{D})$ vanishes. This means that a loop containing a Dirac point cannot be contracted to a point. Indeed, calculating the winding number along such loop, one finds that it is equal to the chirality of the cone $W = \pm 1$. If we then continuously deform the Hamiltonian (always making sure that $\det A$ does not vanish on the loop), since W cannot change, the Dirac cone can only move around, but never gap out. Therefore, we say that the Dirac cone is topologically protected.

In general, the winding number of a loop is equal to the sum of the chiralities of the Dirac points that it encloses, so a loop surrounding two Dirac points with opposite chiralities has $W = 0$. In consequence, pairs of Dirac cones with opposite chiralities can gap each other out without changing W. This means that *only unpaired Dirac cones are protected*.

The winding number can also help us derive the no-go theorem in 2D. The winding number of the loop γ_e that goes along the edges of the Brillouin zone will be equal to the sum of the chiralities of all the Dirac cones in the Brillouin zone.[4] For this loop, the integral (1.5) can be separated into four integrals along each of the edges of the Brillouin zone. Due to the periodicity of $H(\boldsymbol{k})$, these integrals must cancel out by pairs, so the sum of the chiralities of the Dirac points in the BZ is always zero.

[3] In the most general case, A does not need to be a square matrix. In that case, there is always a set of states of fixed chirality pinned to zero energy, and the following discussion must be slightly adapted. Since this is not the case for the Dirac Hamiltonian, we will not get into these details.

[4] If there is a Dirac point on the edges of the Brillouin zone, we can always sligthly deform our path γ_e to avoid it while making sure that the whole BZ is contained in the loop and the argument still applies.

This proves that if the Hamiltonian is local and has chiral symmetry, it cannot have a single unpaired Dirac cone.

Symplectic symmetry

The time reversal symmetry of spinful systems is called symplectic symmetry. If it holds, Kramers theorem applies [10]. This theorem dictates that all eigenstates of the Hamiltonian must be doubly degenerate. Since time reversal maps $\boldsymbol{k} \to -\boldsymbol{k}$, a band crossing is necessary at time reversally invariant momenta (TRIMs) for any local Hamiltonian (namely, continuous in reciprocal space).[5] Therefore, a Dirac cone at a TRIM is protected by symplectic symmetry.

If both chiral and symplectic symmetries are maintained, the Brillouin zone contains a Dirac point at zero energy at each TRIM. There are 2^d such time-reversally invariant momenta in d dimensions, so 4 in 2D. If we then break symplectic symmetry we can move the Dirac points around and gap them out pairwise by merging two Dirac cones with opposite winding number. However, we can not end up with an unpaired Dirac cone unless we also break chiral symmetry, spoiling the topological protection.

In the next section, we review the most commonly used discretization methods for the Dirac Hamiltonian, and in 1.3.5 we introduce the tangent fermions approach which breaks the locality condition to find a work around: a nonlocal discretization can have discontinuities or poles in the dispersion relation, which may "hide" a Dirac point.

1.3. Methods to discretize the Dirac equation

We now turn to the overview of methods to discretize the 2D Dirac Hamiltonian,

$$H_0 = \hbar v(k_x\sigma_x + k_y\sigma_y) = \hbar v \begin{pmatrix} 0 & -i\partial_x - \partial_y \\ -i\partial_x + \partial_y & 0 \end{pmatrix}, \tag{1.6}$$

focusing on the case that the massless electrons can move freely on the x–y plane, without any electromagnetic fields. The Dirac fermions have energy independent velocity v. The Pauli spin matrices $\boldsymbol{\sigma}$ are coupled to the momentum $\boldsymbol{k} = -i\partial_{\boldsymbol{r}}$. In Eq. (1.6) the spin-momentum locking is such that the spin points parallel to the momentum. The alternative

[5] a point $\boldsymbol{k}_T$ of the Brillouin zone is at a TRIM if $2\boldsymbol{k}_T$ is a reciprocal lattice vector.

perpendicular spin-momentum locking ($k_x\sigma_y - k_y\sigma_x$) can be obtained by a unitary transformation of H_0, so we need not distinguish the two cases here.

The energy-momentum relation (dispersion relation) of the Dirac Hamiltonian,

$$E(\boldsymbol{k})^2 = (\hbar v)^2(k_x^2 + k_y^2), \tag{1.7}$$

consists of a pair of cones that touch at the point $\boldsymbol{k} = 0$ — the Dirac point. When the Hamiltonian is discretized on a lattice the dispersion relation becomes periodic: $E(\boldsymbol{k} + \boldsymbol{K}) = E(\boldsymbol{k})$ for any reciprocal lattice vector $\boldsymbol{K}$. Momenta which are not related by a reciprocal lattice vector form the Brillouin zone. For some discretization methods the Dirac point at $\boldsymbol{k} = 0$ is copied at other points in the Brillouin zone (fermion doubling).

The Dirac Hamiltonian (1.6) satisfies the two symmetry relations introduced in the previous section,

$$\begin{aligned} \text{chiral symmetry:}\ & \sigma_z H_0 \sigma_z = -H_0, \\ \text{symplectic symmetry:}\ & \sigma_y H_0^* \sigma_y = H_0. \end{aligned} \tag{1.8}$$

The complex conjugation is taken in the real-space basis, so the sign of both momentum and spin is inverted by the symplectic symmetry operation. For each discretization method we will check whether the symmetries (1.8) are preserved or not.

The topological protection of the Dirac point relies on the absence of fermion doubling and on the conservation of at least one of the two fundamental symmetries (1.8). The linearity of the dispersion relation, $E \propto |\boldsymbol{k}|$, may be a desirable feature, but it is not essential for the protection. What is essential for a practical method is that the eigenvalue problem can be solved using linear algebra of sparse matrices.

In Table 1.1 we summarize the properties of the various discretization schemes that we will discuss. Each discretization has its own dispersion relation, which reduces to the linear dispersion near the physical Dirac point at the center $\boldsymbol{k} = 0$ of the Brillouin zone. The distinguishing properties include:

- the symmetries that the discretization does or does not preserve — the chiral symmetry which defines the handedness of the particles and the symplectic symmetry which is the time-reversal symmetry for spin-1/2 particles;
- the number of Dirac points in the Brillouin zone (1 if there is no fermion doubling);

dispersion	chiral symm.	symplectic symm.	Dirac points	locality	top. prot.
sine	✓	✓	4	✓	×
sine+cosine ([11])	×	×	1	✓	×
staggered ([12])	✓	×	2	✓	×
linear sawtooth ([13])	✓	✓	1	×	×
tangent ([8])	✓	✓	1	×(✓)	✓

Table 1.1: Five approaches to discretize the Dirac equation on a 2D lattice. The presence or absence of a property is indicated by ✓ or ×, respectively. The tangent dispersion has a nonlocal Hamiltonian, but it allows a local formulation of a generalized eigenproblem (hence the ✓ in parentheses). Only the tangent dispersion has an unpaired and topologically protected Dirac point.

- the locality of the discretization, meaning whether the discretized Hamiltonian only couples nearby lattice points;
- and finally the presence or absence of the protection against gap opening by disorder.

1.3.1. Sine dispersion

We start with a square lattice, lattice constant a, and discretize the derivative operator by the first order finite difference:

$$\partial_x f(x,y) \mapsto (2a)^{-1}[f(x+a,y) - f(x-a,y)], \tag{1.9}$$

and similarly for $\partial_y f(x,y)$. Notice that $e^{a\partial_x} = e^{iak_x}$ is the translation operator, $e^{a\partial_x} f(x) = f(x+a)$. The discretization (1.9) therefore gives the Hamiltonian

$$H_{\text{sine}} = (\hbar v/a)(\sigma_x \sin ak_x + \sigma_y \sin ak_y), \tag{1.10}$$

with the sine dispersion

$$E_{\text{sine}}(\boldsymbol{k})^2 = (\hbar v/a)^2(\sin^2 ak_x + \sin^2 ak_y). \tag{1.11}$$

Chiral symmetry and symplectic symmetry (1.8) are both preserved by the Hamiltonian H_{sine}, but there is fermion doubling: In the Brillouin zone $|k_x| < \pi/a$, $|k_y| < \pi/a$ there are Dirac points at each of the time-reversally invariant momenta: the center $\boldsymbol{k} = 0$, the corners $|k_x| = |k_y| = \pi/a$

and the midpoints $k_x = 0, |k_y| = \pi/a$ and $k_y = 0, |k_x| = \pi/a$. The four corners and opposite midpoints are related by a linear combination of reciprocal lattice vectors $\boldsymbol{K} = (2\pi/a, 0)$ and $\boldsymbol{K}' = (0, 2\pi/a)$, so there are 4 inequivalent Dirac points in the Brillouin zone.

1.3.2. Sine plus cosine dispersion

An effective way to remove the spurious Dirac points is to gap them by the addition of a momentum dependent magnetization $\mu(\boldsymbol{k})\sigma_z$ to the Dirac Hamiltonian. If μ vanishes at $\boldsymbol{k} = 0$ the physical Dirac point at the center of the Brillouin zone is unaffected. This is the approach introduced by Wilson [11, 14]. A quadratic $\mu \propto k^2$ is discretized on a square lattice, resulting in the Hamiltonian

$$H_{\text{Wilson}} = (\hbar v/a)(\sigma_x \sin ak_x + \sigma_y \sin ak_y) + m_0\sigma_z(2 - \cos ak_x - \cos ak_y), \tag{1.12}$$

with the sine plus cosine dispersion

$$E_{\text{Wilson}}(\boldsymbol{k})^2 = (\hbar v/a)^2(\sin^2 ak_x + \sin^2 ak_y) + m_0^2(2 - \cos ak_x - \cos ak_y)^2. \tag{1.13}$$

The Dirac points of the sine dispersion acquire a gap $\propto m_0$, only the Dirac point at $\boldsymbol{k} = 0$ remains gapless.

Fermion doubling in Wilson's approach is avoided at expense of a breaking of both chiral and symplectic symmetries. The product of these two symmetries is preserved,

$$\sigma_x H^*_{\text{Wilson}}\sigma_x = -H_{\text{Wilson}}, \tag{1.14}$$

which is sufficient for some applications [15–18].

1.3.3. Staggered lattice dispersion

Much of the particle physics literature follows Susskind's approach [12, 19], which applies a different lattice to each of the two components of the spinor wave function $\Psi = (u, v)$. The two lattices are staggered, see Fig. 1.2, displaced by half a lattice constant. The momentum operator transfers from one lattice to the other, which amounts to a diagonal displacement by a distance of $a/\sqrt{2}$, as expressed by the translation operators $e^{ia(k_x \pm k_y)/2}$.

The discretized Dirac Hamiltonian still acts on the original lattice (black

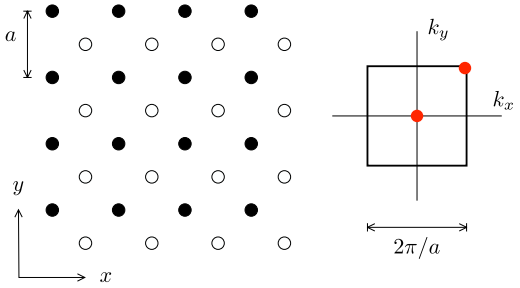

Figure 1.2: Left: Staggered pair of grids for the discretization of Dirac fermions in Susskind's approach. The black and white dots distinguish the u and v amplitudes of the spinor wave function $\Psi = (u, v)$. Right: The square shows the Brillouin zone in momentum space, the red dots indicate two inequivalent Dirac points.

dots in Fig. 3.1). The unitary transformation with operator

$$U_{\text{stagger}} = \begin{pmatrix} 1 & 0 \\ 0 & e^{ia(k_x+k_y)/2} \end{pmatrix} \tag{1.15}$$

initializes the pair of staggered lattices (u component on the black dots, v-component on the white dots). The Hamiltonian then takes the form

$$H_{\text{Susskind}} = \sqrt{2}\frac{\hbar v}{a} U^{\dagger}_{\text{stagg.}} \big(\sigma_x \sin[a(k_x - k_y)/2] + \sigma_y \sin[a(k_x + k_y)/2]\big) U_{\text{stagg.}}. \tag{1.16}$$

Check that the $2\pi/a$ periodicity in the k_x and k_y components is maintained: the minus sign picked up by the sine terms is canceled by the unitaries.

In terms of the rotated momenta $q_x = (k_x - k_y)/\sqrt{2}$, $q_y = (k_x + k_y)/\sqrt{2}$, normalized such that $|\boldsymbol{q}|^2 = |\boldsymbol{k}|^2$, one has

$$H_{\text{Susskind}} = \hbar v[q_x \sigma_x + q_y \sigma_y + \mathcal{O}(q^2)], \tag{1.17}$$

so the Dirac Hamiltonian (1.6) is recovered in the continuum limit.

The corresponding dispersion relation

$$E_{\text{Susskind}}(\boldsymbol{k})^2 = 2(\hbar v/a)^2 \big(\sin^2[(k_x - k_y)/2] + \sin^2[(k_x + k_y)/2]\big) \tag{1.18}$$

has two inequivalent Dirac points in the Brillouin zone, at the center and at the corner. Compared to the sine discretization the staggered lattice has reduced the number of Dirac points from four to two, but fermion

doubling has not been fully eliminated. Chiral symmetry is preserved, but symplectic symmetry is broken by the relative displacement of the two spinor components.

More generally, on a d-dimensional lattice the sine dispersion has 2^d inequivalent Dirac points in the Brillouin zone (one at each time-reversally invariant momentum), and the staggered lattice reduces that by one half. For $d = 1$ this is sufficient to avoid fermion doubling. In that case the Susskind Hamiltonian (1.16) is equivalent (up to a unitary transformation) to the 1D Wilson Hamiltonian

$$H_{\text{Wilson}}(k_x, k_y = 0) = (\hbar v/a)\sigma_x \sin ak_x + m_0\sigma_z(1 - \cos ak_x) \tag{1.19}$$

for the special value $m_0 = \hbar v/a$. The resulting $\sin(ak_x/2)$ dispersion is shown in Fig. 1.3 (green curve).

1.3.4. Linear sawtooth dispersion

The discretization schemes discussed in the previous subsection are all local, in the sense that they produce a sparse Hamiltonian: each lattice site is only coupled to a few neighbors. If one is willing to abandon the locality of the Hamiltonian, one can eliminate the fermion doubling by a discretization of the spatial derivative that involves all lattice points,

$$\begin{aligned}\partial_x f(x,y) &\mapsto a^{-1}\sum_{n=1}^{\infty}(-1)^n n^{-1}[f(x-na,y) - f(x+na,y)] \\ &= a^{-1}\sum_{n=1}^{\infty}(-1)^n n^{-1}(e^{-na\partial_x} - e^{na\partial_x})f(x,y) = a^{-1}(\ln e^{a\partial_x})f(x,y).\end{aligned} \tag{1.20}$$

This discretization scheme goes by the name of SLAC fermions [13, 20] in the particle physics literature. It has also been implemented in a condensed matter context [21–24].

In momentum representation, the Hamiltonian takes the form

$$H_{\text{SLAC}} = -i(\hbar v/a)\big(\sigma_x \ln e^{iak_x} + \sigma_y \ln e^{iak_y}\big), \tag{1.21}$$

where the branch cut of the logarithm is taken on the negative real axis. The corresponding dispersion

$$E_{\text{SLAC}}(\boldsymbol{k})^2 = (\hbar v)^2\,(k_x^2 + k_y^2) \quad \text{for} \quad |k_x|, |k_y| < \pi/a, \tag{1.22}$$

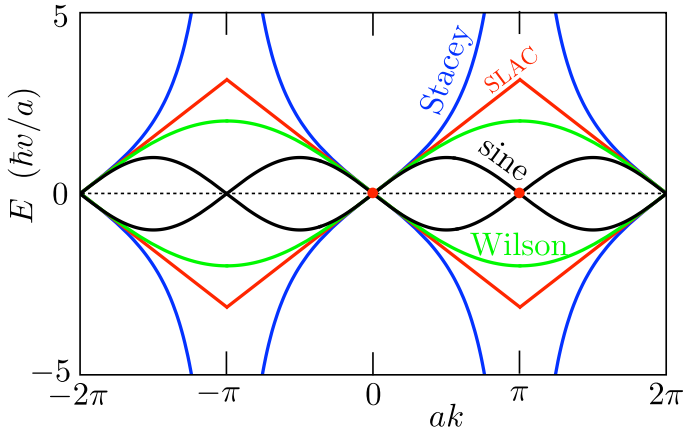

Figure 1.3: Dispersion relations of Dirac fermions on a 1D lattice, for four different discretization schemes. One with fermion doubling (black curve, E_{sine}) and three without fermion doubling: E_{Wilson} (green curve, for $m_0 = \hbar v/a$, when $E_{\text{Susskind}} = E_{\text{Wilson}}$), E_{SLAC} (red curve), and E_{Stacey} (blue curve). Inequivalent Dirac points are indicated by a red dot. The first Brillouin zone is the interval $|k| < \pi/a$, the plot is extended to $|k| < 2\pi/a$ to show the dispersion on both sides of the Brillouin zone boundary.

is a linear sawtooth, with a cusp at the edge of the Brillouin zone (see Fig. 1.3, red curve). Fermion doubling is avoided and both chiral and symplectic symmetries are preserved.

1.3.5. Tangent dispersion

The approach pioneered by Stacey [8, 25] seems a minor modification of the SLAC approach — but it has far reaching consequences. The nonlocal derivative (1.20) is modified by removal of the $1/n$ factor,

$$\begin{aligned}\partial_x f(x,y) &\mapsto 2a^{-1}\sum_{n=1}^{\infty}(-1)^n[f(x-na,y)-f(x+na,y)]\\ &= 2a^{-1}\sum_{n}(-1)^n(e^{-na\partial_x}-e^{na\partial_x})f(x,y)\\ &= -(2i/a)\tan(ia\partial_x/2)f(x,y).\end{aligned} \tag{1.23}$$

The corresponding Hamiltonian

$$H_{\text{Stacey}} = (2\hbar v/a)\big[\sigma_x \tan(ak_x/2) + \sigma_y \tan(ak_y/2)\big], \tag{1.24}$$

has a tangent dispersion,

$$E_{\text{Stacey}}(\boldsymbol{k})^2 = (2\hbar v/a)^2 \left[\tan^2(ak_x/2) + \tan^2(ak_y/2)\right]. \tag{1.25}$$

The cusp at the Brillouin zone boundary has been replaced by a pole (see Fig. 1.3, blue curve).

As in the SLAC approach, the Stacey approach avoids fermion doubling while preserving chiral and symplectic symmetries, at the expense of a nonlocal Hamiltonian. The key merit of the tangent dispersion is that the nonlocality can be removed by transforming the eigenproblem $H\Psi = E\Psi$ into a generalized eigenproblem $\mathcal{H}\Psi = E\mathcal{P}\Psi$, with local operators $\mathcal{H}$ and $\mathcal{P}$ on both sides of the equation. This transformation is possible because the tangent is the ratio of two operators, sine and cosine, that have a local representation on the lattice.

Ref. [8] formulated the generalized eigenproblem by means of finite differences on a pair of staggered grids. This produces operators $\mathcal{H}$ and $\mathcal{P}$ that are local but not Hermitian, which is problematic in a numerical implementation. The alternative formulation of Ref. [26] resolves this issue, resulting in the generalized eigenproblem

$$\begin{aligned} &\mathcal{H}\Psi = E\mathcal{P}\Psi, \quad \mathcal{P} = \tfrac{1}{4}(1+\cos ak_x)(1+\cos ak_y), \\ &\mathcal{H} = \frac{\hbar v}{2a}\big[\sigma_x(1+\cos ak_y)\sin ak_x + \sigma_y(1+\cos ak_x)\sin ak_y\big]. \end{aligned} \tag{1.26}$$

Both operators $\mathcal{H}$ and $\mathcal{P}$ are Hermitian and $\mathcal{P}$ is also positive definite.[6] Both are sparse matrices, only nearby sites on the lattice are coupled. This combination of properties allows for an efficient calculation of the energy spectrum. In order to do this in practice, it is essential to formulate this problem in real space.

[6] To avoid the complications from a noninvertible $\mathcal{P}$, one can choose a lattice with periodic boundary conditions over an odd number of sites; then all eigenvalues of $\mathcal{P}$ are strictly positive.

Real-space formulation of the generalized eigenproblem.

The generalized eigenproblem (1.26) of tangent fermions can be formulated in the position basis upon the substitution

$$e^{iak_\alpha} \mapsto \sum_{\boldsymbol{n}} |\boldsymbol{n}\rangle\langle\boldsymbol{n}+\boldsymbol{e}_\alpha|. \tag{1.27}$$

The sum over $\boldsymbol{n} = n_x\boldsymbol{e}_x + n_y\boldsymbol{e}_y$, with $n_x, n_y \in \mathbb{Z}$, is a sum over lattice sites on the 2D square lattice (lattice constant a).

We thus have the equation $\mathcal{H}\Psi = E\mathcal{P}\Psi$, with on the left-hand-side the operator

$$\mathcal{H} = -\frac{i\hbar v}{a}\boldsymbol{D}\cdot\boldsymbol{\sigma}, \quad \boldsymbol{D} = (D_x, D_y), \tag{1.28a}$$

$$D_x = \tfrac{1}{8}\sum_{\boldsymbol{n}}\Big(2|\boldsymbol{n}\rangle\langle\boldsymbol{n}+\boldsymbol{e}_x| + |\boldsymbol{n}\rangle\langle\boldsymbol{n}+\boldsymbol{e}_x+\boldsymbol{e}_y| + |\boldsymbol{n}\rangle\langle\boldsymbol{n}+\boldsymbol{e}_x-\boldsymbol{e}_y|\Big) - \text{H.c.}, \tag{1.28b}$$

$$D_y = \tfrac{1}{8}\sum_{\boldsymbol{n}}\Big(2|\boldsymbol{n}\rangle\langle\boldsymbol{n}+\boldsymbol{e}_y| + |\boldsymbol{n}\rangle\langle\boldsymbol{n}+\boldsymbol{e}_x+\boldsymbol{e}_y| + |\boldsymbol{n}\rangle\langle\boldsymbol{n}+\boldsymbol{e}_y-\boldsymbol{e}_x|\Big) - \text{H.c.}, \tag{1.28c}$$

and on the right-hand-side the operator $\mathcal{P} = \Phi^\dagger\Phi$ with

$$\Phi = \tfrac{1}{4}\sum_{\boldsymbol{n}}\Big(|\boldsymbol{n}\rangle\langle\boldsymbol{n}| + |\boldsymbol{n}\rangle\langle\boldsymbol{n}+\boldsymbol{e}_x| + |\boldsymbol{n}\rangle\langle\boldsymbol{n}+\boldsymbol{e}_y| + |\boldsymbol{n}\rangle\langle\boldsymbol{n}+\boldsymbol{e}_x+\boldsymbol{e}_y|\Big). \tag{1.29}$$

The abbreviation H.c. stands for "Hermitian conjugate". Both operators $\mathcal{H}$ and $\mathcal{P}$ are local, only nearby lattice points are connected.

By way of illustration, we work out the expectation value

$$\langle\psi|\Phi^\dagger\Phi|\psi\rangle = \sum_{\boldsymbol{n}}|\tilde{\psi}_{\boldsymbol{n}}|^2, \quad \tilde{\psi}_{\boldsymbol{n}} = \tfrac{1}{4}(\psi_{\boldsymbol{n}}+\psi_{\boldsymbol{n}+\boldsymbol{e}_x}+\psi_{\boldsymbol{n}+\boldsymbol{e}_y}+\psi_{\boldsymbol{n}+\boldsymbol{e}_x+\boldsymbol{e}_y}). \tag{1.30}$$

One can interpret this in terms of the two staggered lattices shown in Fig. 1.4. The field $\tilde{\psi} = \Phi\psi$ is defined on a white lattice point as the average of the amplitudes of the wave function ψ on the four adjacent black lattice points.

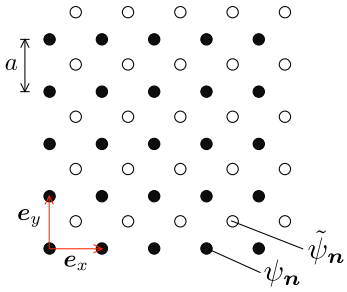

Figure 1.4: Staggered pair of grids to represent the two fields ψ and $\tilde{\psi} = \Phi\psi$. *Figure from Ref. [26].*

1.4. Chiral superconductors

As shown by Fu and Kane, a 3DTI can be used to engineer a chiral superconductor [27] by proximitizing it with an s-wave superconductor. The Bogoliubov-de Gennes Hamiltonian corresponding to such system is

$$H = \begin{pmatrix} \hbar v \boldsymbol{k}\cdot\boldsymbol{\sigma} - \mu & \Delta^* \\ \Delta & -\hbar v \boldsymbol{k}\cdot\boldsymbol{\sigma} + \mu \end{pmatrix}. \tag{1.31}$$

The unitary transformation given by

$$U = \begin{pmatrix} \exp\left(-i\frac{\pi}{4}(\sin\theta_k\sigma_x - \cos\theta_k\sigma_y)\right) & 0 \\ 0 & \exp\left(i\frac{\pi}{4}(\sin\theta_k\sigma_x - \cos\theta_k\sigma_y)\right) \end{pmatrix}, \tag{1.32}$$

being θ_k the polar angle of $\boldsymbol{k}$, transforms our Hamiltonian into

$$UHU^\dagger = \begin{pmatrix} \hbar v|\boldsymbol{k}| - \mu & 0 & 0 & \Delta^* e^{-i\theta_k} \\ 0 & -\hbar v|\boldsymbol{k}| - \mu & -\Delta^* e^{i\theta_k} & \\ 0 & -\Delta e^{-i\theta_k} & \hbar v|\boldsymbol{k}| + \mu & 0 \\ \Delta e^{i\theta_k} & 0 & 0 & -\hbar v|\boldsymbol{k}| + \mu \end{pmatrix}. \tag{1.33}$$

For $\mu \gg |\Delta|$, the low energy spectrum is given by the first and fourth blocks, so we can project on them to obtain

$$H_C = \begin{pmatrix} \hbar v|\boldsymbol{k}| - \mu & \Delta^* e^{-i\theta_k} \\ \Delta e^{i\theta_k} & -\hbar v|\boldsymbol{k}| + \mu \end{pmatrix}. \tag{1.34}$$

Since the superconducting phase along the normal Fermi surface winds once, this effective Hamiltonian realises a chiral superconductor. These

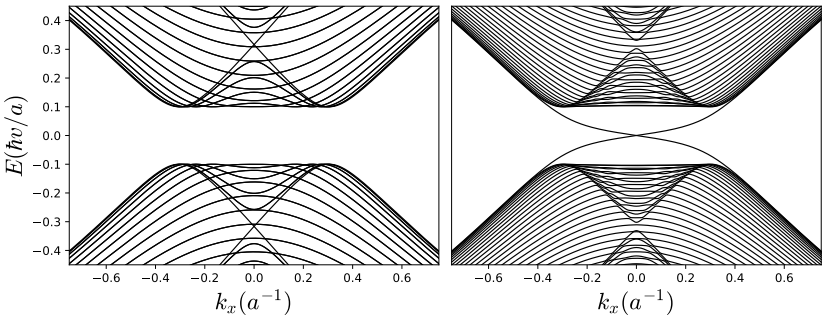

Figure 1.5: Low energy band structure in x direction of a tight-binding version of the Hamiltonian 1.31 for a periodic system in y direction (left) and a finite system with magnetic boundaries (right). In the finite system, we can appreciate two gapless edge modes with opposite velocity. The boundaries also lift the degeneracy of the bulk bands.

systems are topological [28], and they can host chiral edge modes. This is only possible if time reversal symmetry is broken. Since Hamiltonian 1.31 does not break it, the boundaries must. This is achieved by a magnetization term in z direction. The corresponding band structure is shown in Fig. 1.5.

In [29], they used this realisation of a chiral superconductor to observe the gap closing caused by a net superconducting current [30]. This happens due to the Doppler shift δE of the bands $\varepsilon(\boldsymbol{p})$ caused by the Cooper pair momentum $\boldsymbol{p}_s$ [31],

$$\delta E(\boldsymbol{p}) = \boldsymbol{p}_s \cdot \frac{\partial \varepsilon(\boldsymbol{p})}{\partial \boldsymbol{p}}. \tag{1.35}$$

In chapter 5, we study the effect of a net supercurrent on the chiral edge modes of such system.

1.5. Non-abelian anyons and braiding

A fundamental property that distinguishes fermions from bosons is their *exchange statistics*. This term refers to how the state of a system transforms when two particles are exchanged. We can express it as

$$|\Psi_{21}\rangle = U\,|\Psi_{21}\rangle\,. \tag{1.36}$$

For fermions the wavefunction changes sign, $U = -1$, while for bosons it stays the same, $U = 1$. A detail that is often overlooked in this regard is the fact that we can mean two different things by "particle exchange" [32]. On one hand, we can switch the quantum numbers of two particles. The statistics of fermions under this notion of exchange is responsible for the Pauli exclusion principle.

On the other hand, we can think of exchanging two particles by adiabatically driving them to each other's position without encountering each other along the way. In 3D, the Berry phase associated to such an exchange can only take the values ± 1, corresponding to bosons and fermions respectively. However, in 2D there can exist particles that acquire any phase.[7] We call this particles anyons, and for them $U = e^{i\theta}$.

If the ground state of a 2D system with two particles is degenerate, there is still a more general scenario. In such case, it is possible for the exchange to produce a linearly independent state. Particles with this behavior are called non-Abelian anyons and their exchange is described by a unitary transformation U rather than just a phase.

Kitaev managed to show how this property can be exploited to build a fault-tolerant quantum computer [33]. The idea is to encode a set of qubits in the ground state of a system of non-Abelian quasiparticles and use exchange operations to implement quantum gates on them. The world lines of the quasiparticles during this process interlace each other, and every possible braid results in a specific unitary transformation, hence the term *non-abelian braiding*. These systems store information non-locally and this makes the process immune to decoherence.

The first physical systems found to host non-Abelian anyons were fractional quantum Hall states at some specific filling factors (e.g. $\nu = 5/2$) [34, 35], but recently more attention has been given to topological superconductors like the ones described in the previous section. A $\varphi = h/2e$ magnetic flux tube threading a 2D topological superconductor creates an Abrikosov vortex in the superconducting pairing that binds a zero energy state. This state is called Majorana zero mode (MZM) because it is its own particle-hole partner.

A qubit can be encoded in the parity of two MZMs, i.e. in the filling of the fermionic degree of freedom that is split between them. Since the total parity of a superconductor is fixed, the minimal example of braiding with MZMs requires two pairs of these quasiparticles. Braiding one MZM from the first pair around another from the other pair induces a transfer

[7] The reason behind this difference comes down to the fact that in the 2D space, a loop around the origin cannot be contracted to a point without crossing it, while in 3D this can be done by lifting up the loop in the third dimension.

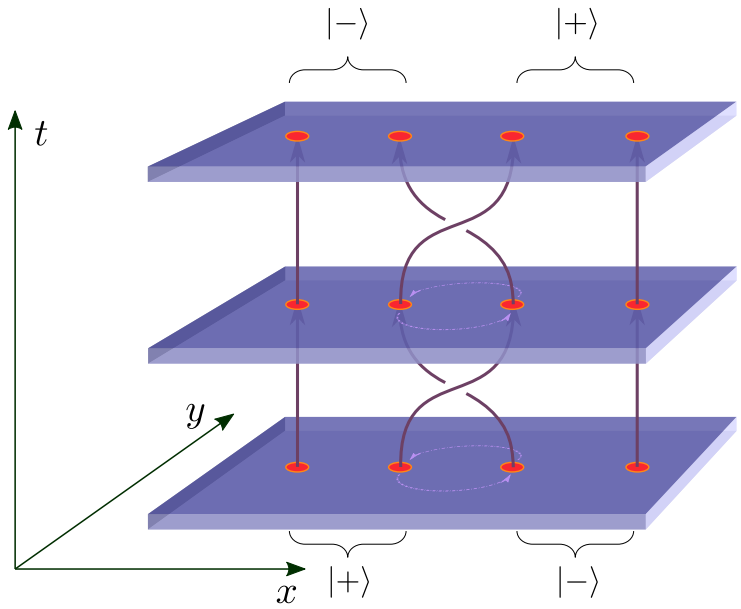

Figure 1.6: Schematics of the implementation of a σ_x gate on the state $\psi_{\text{in}} = |+\rangle|-\rangle$ to turn it into $\psi_{\text{out}} = |-\rangle|+\rangle$.

of a fermion between the pairs. This transformation corresponds to a σ_x gate (see [36]). A measurement of the state can be carried out by fusing a pair and measuring the corresponding parity.

A big obstacle stands in the way of implementing this protocol in practice, namely the fact that adiabatically moving around individual Abrikosov vortices is beyond our current technical capabilities. Fortunately, another kind of non-Abelian quasiparticles that can exist on the chiral edges of topological superconductors provides us with a solution. We are not referring to the ordinary edge Majorana fermions, which are Bogoliubov excitations with fermionic statistics, but to a special kind of many-body excitation called *edge-vortex*. They consist of a π-phase kink on the Majorana edge ground state, which is stable due to the reality condition of Majorana wavefunctions [37]. These excitations have non-Abelian statistics and they propagate along the edge of the superconductor at the edge mode velocity.

In chapter 6, we demonstrate a protocol to inject, braid and fuse edge vortices proposed by Beenakker *et al.* [38]. Although we model the

process with a proximitised Chern insulator, a proximitised 3DTI surface surrounded by magnetic regions with opposite magnetizations would realise the same low energy phenomenology.

1.6. This thesis

Although the overarching theme of this thesis falls within the topic of lattice massless fermions, two distinct parts can be established. Chapters 2, 3 and 4 are devoted to developing various aspects of the *tangent fermions* discretization method, such as the implementation of time evolution or the inclusion of a magnetic field in a gauge invariant way. In contrast, chapters 5 and 6 study specific phenomena associated to chiral superconductors, using both analytical and numerical methods.

Chapter 2

As discussed in section 1.2, symmetries are crucial for the topological protection of a single Dirac cone. However, they will only provide such protection if the Hamiltonian is continuous in the whole reciprocal space, including across the edges of the Brillouin zone. This is often overlooked in many discretization methods.

In this chapter, we introduce a way to solve the time-dependent Dirac equation for massless fermions on a lattice that is discrete not only in space but also in time. The resulting evolution operator has unique properties. It preserves chiral and symplectic symmetries, it avoids fermion doubling and, remarkably, it is continuous across the edge of the energy-momentum Brillouin zone. We explicitly show how other methods fail to keep the gaplessness of the Dirac cone while in ours it is robust against any chiral or symplectic symmetry preserving perturbations. Since our dispersion relation reads $\tan^2(\varepsilon/2) = \tan^2(k_x/2) + \tan^2(k_y/2)$, we refer to our approach as the method of *tangent fermions*.

Chapter 3

Apart from the robustness of the Dirac cone, another well known property of massless fermions is a phenomenon known as “Klein tunneling”. It consists on the impossibility of backscattering of electrons that encounter a potential step perpendicular to their direction of motion, irrespective of the size of the barrier. This happens because such backscattering would

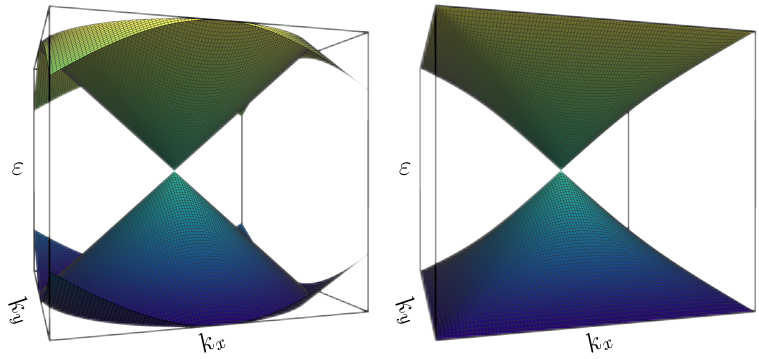

Figure 1.7: Band structure for SLAC (left) and tangent fermions (right). The bands are discontinuous accross the edge of the Brillouin zone only in the former.

require a spin switch, which is forbidden in chiral symmetry preserving systems.

However, this phenomenon may be spoiled by fermion doubling because of scattering to another Dirac cones in the Brillouin zone. To avoid this, a staggered space-time lattice discretization has been developed in the literature, with *one* single Dirac cone in the Brillouin zone of the original square lattice. In this chapter we show that the staggering doubles the size of the Brillouin zone, which actually contains *two* Dirac cones. We find that this fermion doubling causes a spurious breakdown of Klein tunneling, which can be avoided by the alternative single-cone discretization scheme introduced in chapter 2.

Chapter 4

The presence of a magnetic field B in a system of fermions induces Landau quantization, a phenomenon consisting on the emergence of separate flat energy bands known as Landau levels. While this happens for both massive and massless fermions, in the latter case the spectrum contains a particular Landau level at zero energy that is absent in the former. This "zeroth Landau level" is special because it has a well defined chirality, which makes its flatness robust against chirality preserving disorder.

However, a lattice discretization with fermion doubling or chiral symmetry breaking can spoil this protection, inducing a broadening of the zeroth Landau level when B has spatial fluctuations. In this chapter, we

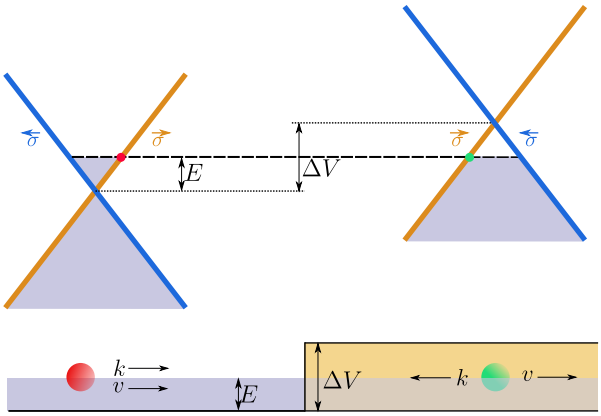

Figure 1.8: Klein tunneling. The incoming electron (red) can only be transmitted, switching its momentum and keeping its spin and velocity (green).

extend the tangent fermions approach to allow for the incorporation of magnetic fields and show how this can be used to obtain robust zeroth Landau levels.

Chapter 5

The right panel of Fig. 1.5 shows the band structure of a spinful chiral superconductor –more specifically, a Fu-Kane heterostructure– for zero supercurrent. In this chapter we explore the effect a non-zero net supercurrent parallel to the edges of such system and find out that something special happens at a critical value of the Cooper pair momentum $\Delta_0^2/\mu v_F$. At this point, the velocity of one of the Majorana edge modes switches sign –we call this a *chirality inversion*–, a process that is accompanied by the emergence of two new states at the Fermi energy.

This chirality inversion leaves traces in the transport properties of the system. Firstly, the heat conductance is doubled because now there are twice as many modes that can transport energy. Secondly, the newly generated modes have non-zero charge, so electrical current can now be transported, and therefore the system acquires a non-zero electrical conductance. We also show that the chirality inversion is a unique signature of Majorana fermions in a spinful topological superconductor: it does not exist for spinless chiral p-wave pairing.

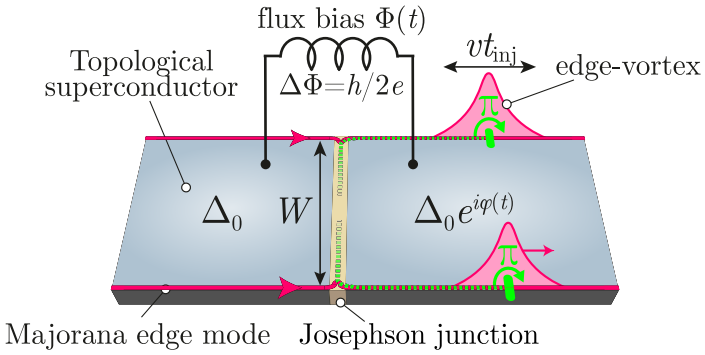

Figure 1.9: Edge vortex injector of [38].

Chapter 6

As introduced in section 1.5, the chiral edge modes of a topological superconductor can carry non-Abelian excitations. These so-called edge-vortices are a π-phase "twist" of the wavefunctions of the edge Bogoliubov quasiparticles below the Fermi energy. These many-body excitations are made up of chiral edge modes which propagate along the edge of the system at the same velocity. Therefore, edge-vortices themselves must do the same.

In [38], Beenakker *et al.* proposed that such edge-vortices can be injected on the edges of a topological superconductor by splitting it with a Josephson junction and applying an $h/2e$ flux bias over it. In this chapter, we demonstrate it by dynamically simulating the process using a lattice model. Essentially, this amounts to numerically solving the time-dependent Schrödinger equation for the ground state of the superconducting device.

We show how the braiding of edge-vortices with bulk vortices results in a parity switch analogous to the one represented in Fig. 1.6. We also confirm the prediction made in [38] that the braiding process can be detected electrically. More crucially, our approach allows us to account for the dynamics of the junction and go beyond exisiting analytic descriptions that rely on the adiabatic approximation. Our study also reveals that if the flux bias is implemented too fast, residual excitations can remain trapped in the Josephson junction, spoiling the parity switch.